

High-energy transient gas pinholes via saturated absorption

K. Ou,^{1,*} V. M. Perez-Ramirez,¹ S. Cao,¹ C. Redshaw,¹ J. Lee,¹ M. Wang,² J. M. Mikhailova,³ P. Michel,⁴ and M. R. Edwards^{1,†}

¹*Department of Mechanical Engineering, Stanford University, Stanford, California 94305*

²*Department of Electrical and Computer Engineering, Princeton University, Princeton, New Jersey 08540*

³*Department of Mechanical and Aerospace Engineering, Princeton University, Princeton, New Jersey 08540*

⁴*Lawrence Livermore National Laboratory, Livermore, California 94551*

(Dated: December 5, 2024)

This letter presents a spatial filter based on saturated absorption in gas as a replacement for the solid pinhole in a lens-pinhole-lens filtering system. We show that an ultraviolet laser pulse focused through ozone will have its spatial profile cleaned if its peak fluence rises above the ozone saturation fluence. Specifically, we demonstrate that a 5 ns 266 nm beam with 4.2 mJ of initial energy can be effectively cleaned by focusing through a 1.4% ozone-oxygen mixture, with about 76% of the main beam energy transmitted and 89% of the side lobe energy absorbed. This process can be adapted to other gases and laser wavelengths, providing alignment-insensitive and damage-resistant pinholes for high-repetition-rate high-energy lasers.

Substantial efforts have been made to control and improve the spatial profiles of high-energy lasers [1–5], since the focusability of a beam depends strongly on its spatial quality. Consequently, spatial filters play a critical role in modern laser systems, used to remove high-frequency spatial noise and clean beam profiles. Filters also reduce diffraction ripples and suppress noise from parasitic lasing, amplified spontaneous emission, and self-focusing [2–4]. A typical spatial filter consists of a lens pair and a solid pinhole, where the latter removes high-frequency components of a beam by physically blocking them at the focal plane. However, this approach becomes challenging to implement when the laser is intense enough to damage the pinhole. In addition, conventional filters require precise alignment and can be vulnerable to vibrations or pointing instability.

In addition to solid pinholes, nonlinear media have been suggested for spatial filtering because the side lobes of a beam have lower intensity than the main peak, so an intensity-dependent response at the focal plane can be used to remove high-frequency components. Nonlinear mechanisms for profile cleaning include harmonic generation [6], ionization [7], and light-induced molecular orientation [8]. An alternative approach is to use saturated absorption of light in nonlinear materials, where absorption drops significantly when beam fluence rises above the saturation threshold. Previous studies have successfully used dye cells to clean lasers with intensity up to 10^{10} W/cm² [9, 10].

In this work, we propose the use of gas as a saturated absorber for spatial filtering. Gases, compared to solid or liquid materials, have orders-of-magnitudes-higher damage thresholds. Recent work has demonstrated the cre-

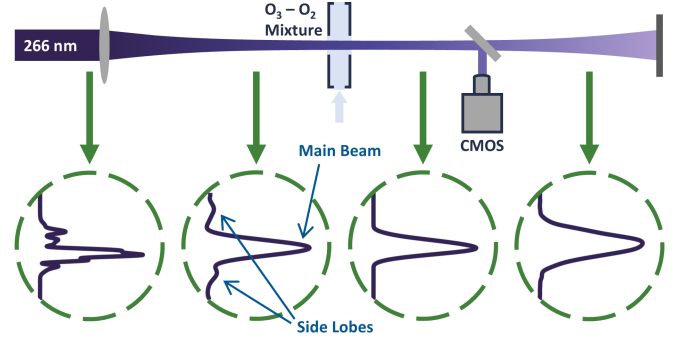


FIG. 1. Experimental schematic. An aberrated 266 nm beam is focused into ozone. By carefully choosing the focal length, tube width, and ozone concentration, the spatially separated high-frequency components at the focal plane are mostly absorbed while the main beam is only mildly attenuated due to saturated absorption, resulting in a cleaner beam profile.

ation of optics like diffraction gratings in gases, with effective damage thresholds expected to be ~ 1 kJ/cm² [11, 12]. Here, we demonstrate the ability of ozone to clean ultraviolet (UV) beams via simulations and experiments. As shown in Fig. 1, a 266 nm laser focused into ozone will exhibit a substantially cleaner profile after exiting the flow. Compared to other spatial filtering techniques, a gas pinhole is relatively straightforward to build, does not require precise alignment, and constantly renews itself. The last feature is a unique advantage, making this design particularly useful for high-energy lasers running at a high repetition rate.

The propagation of a pulsed laser in a saturable absorber can be described by the equations [12, 13]:

$$\frac{\partial I(z, t)}{\partial z} = -\sigma n(z, t)I(z, t) \quad (1)$$

* ouke025@stanford.edu

† mredwards@stanford.edu

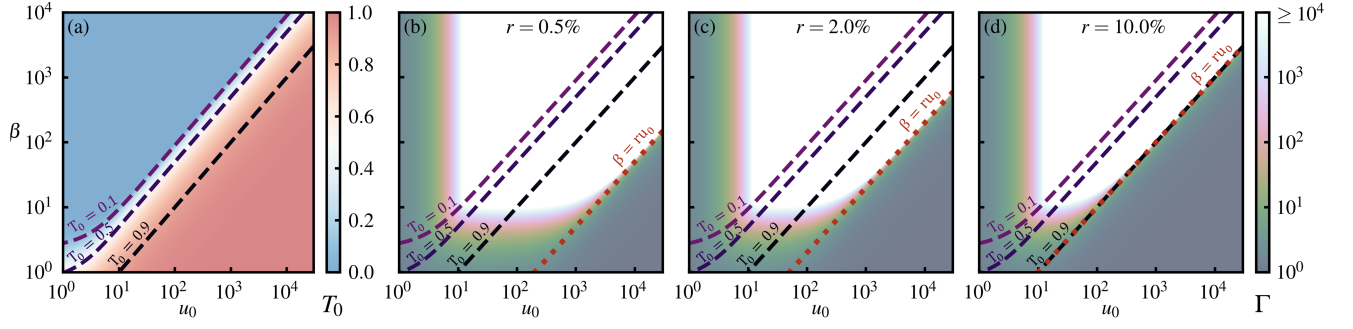


FIG. 2. Transmittance T_0 (a) and noise attenuation Γ (b)-(d) with various normalized fluence u_0 and triple product β at $r = 0.5\%$, 2% and 10% . The dashed contours indicate where T_0 reaches 0.1, 0.5, and 0.9. The dotted contours indicate where $\beta = ru_0$.

$$\frac{\partial n(z, t)}{\partial t} = -\frac{\sigma}{\hbar\omega} n(z, t) I(z, t) \quad (2)$$

Here, I is the laser intensity, n is the number density of saturable absorber molecules, σ is the absorption cross section, \hbar is the reduced Planck's constant, ω is the angular frequency of the light, and z and t are the position and time in a reference frame that moves with the pulse (i.e. $z = \hat{z}$, $t = \hat{t} - \hat{z}/c$ where \hat{z} and \hat{t} are the laboratory frame position and time, and c is the speed of light). To find the density of the absorbing gas species after the pulse propagation, we can integrate (2) over the pulse duration τ :

$$n(z, t > \tau) = n(z, 0) \exp \left[-\frac{\sigma}{\hbar\omega} \int_0^\tau I(z, t) dt \right] = n_0 e^{-U/U_s} \quad (3)$$

where we assume an initially uniform absorber density n_0 , U is the beam fluence, and $U_s \equiv \hbar\omega/\sigma$ is the saturation fluence. Substituting (2) into (1) and integrating over the pulse duration, we obtain:

$$\frac{du}{dz} = \sigma n_0 (e^{-u} - 1) \quad (4)$$

where $u(z) \equiv U(z)/U_s$ is the normalized fluence. Finally, integrating (4), we get:

$$\frac{e^{u(z)} - 1}{e^{u(0)} - 1} = e^{-\sigma n_0 z} \quad (5)$$

If the peak and side lobes of a beam at focus have initial fluences u_0 and u_1 , respectively, the transmittance $T = u(L)/u(0)$ of the two components, after propagation through a gas pinhole of length L will, according to (5), satisfy:

$$\frac{e^{T_0 u_0} - 1}{e^{u_0} - 1} = \frac{e^{T_1 u_1} - 1}{e^{u_1} - 1} = e^{-\beta} \quad (6)$$

with $\beta \equiv \sigma n_0 L$ defined as the triple product of the gas pinhole. Equation 6 implies that changing the absorption cross-section, the number density, or the length of the gas pinhole are equivalent. Let $u_1 = ru_0$ where r is analogous to the inverse of a signal-to-noise ratio that quantifies

the noisiness of a beam. In practice, we can estimate r by taking the Fourier transform of the beam profile and examining the ratio of the central mode amplitude to those of the higher-order modes. Defining the noise attenuation ratio as $\Gamma \equiv T_0/T_1$, Equation 6 can then be written as:

$$\frac{e^{T_0 u_0} - 1}{e^{u_0} - 1} = \frac{e^{\frac{r T_0}{\Gamma} u_0} - 1}{e^{r u_0} - 1} = e^{-\beta} \quad (7)$$

For an ideal gas pinhole, we would like the main beam to be entirely transmitted (i.e. $T_0 \rightarrow 1$) and the side lobes to be completely suppressed ($T_1 \rightarrow 0$ or $\Gamma \rightarrow \infty$). Given properties of the beam and gas pinhole u_0 , r , and β , we can solve for T_0 and Γ from (7):

$$T_0 = \frac{-\beta + \ln(e^\beta + e^{u_0} - 1)}{u_0} \quad (8)$$

$$\Gamma = \frac{r [-\beta + \ln(e^\beta + e^{u_0} - 1)]}{-\beta + \ln(e^\beta + e^{r u_0} - 1)} \quad (9)$$

Figure 2 shows the transmittance T_0 and noise attenuation ratio Γ of a gas pinhole for various initial fluence u_0 and triple product β at $r = 0.5\%$, 2% , and 10% . Unlike traditional spatial filters, the transmittance of a gas pinhole is fluence-dependent. Attenuation is also limited by the beam noisiness, r . As $r \rightarrow 1$, $\Gamma \rightarrow 1$, indicating that spatial cleaning with a gas pinhole becomes impossible. An effective gas pinhole ($T_0 \approx 1$, $\Gamma \gg 1$) requires $u_0 > \beta$ for good transmission, $\beta > ru_0$ for good noise attenuation, and peak fluences well above the saturation fluence, leading to a useful operating regime where

$$u_0 > \beta > ru_0 \gg 1 \quad (10)$$

This condition generally gives $e^{u_0} \gg e^\beta \gg e^{r u_0} \gg 1$, allowing simplification of (8) and (9) to $T_0 \approx 1 - r - \Delta\beta/u_0$ and $\Gamma \approx ru_0 T_0 e^{\Delta\beta}$, where $\Delta\beta = \beta - ru_0 > 0$. There is therefore a trade-off between high T_0 and high Γ . The minimum u_0 depends on the the maximum achievable waist size while the maximum u_0 is limited by how tightly a beam can be focused and the nonlinear threshold of the

gas. The feasibility of a gas pinhole depends on whether a triple product that satisfies (10) can be produced.

We first validated this process with numerical simulations in which a beam propagates through an absorptive medium modeled by a fluence-dependent imaginary refractive index. The simulation also captures the change of the fluence as a beam propagates. Propagation of a paraxial wave in matter is governed by:

$$\left[\nabla_{\perp}^2 + 2ik_0 \partial_z \right] \mathbf{E}(\mathbf{r}) = -2k_0^2 \mathbf{E}(\mathbf{r}) \frac{\delta n(\mathbf{r})}{n_0} \quad (11)$$

where \mathbf{E} is the electric field, k_0 is the vacuum wavenumber, and n_0 and δn are the background and change of the refractive index. The wave equation is solved numerically using a Strang splitting scheme, with each step along z combining the solutions from the paraxial propagation in vacuum via a Fourier transform along x and y [14] and the absorption step, leading to:

$$E(x, y, z_{j+1}) = \mathcal{F}^{-1} \left\{ \mathcal{F} [E(x, y, z_j)] \exp \left(-\frac{ik_{\perp}^2}{2k_0} \Delta z \right) \right\} \times \exp \left[ik_0 \frac{\delta n(x, y, z_j)}{n_0} \Delta z \right] \quad (12)$$

where \mathcal{F} indicates Fourier transform, k_{\perp} is the transverse wavenumber, Δz is the propagation step size, and j is the step number. Without loss of generality, we can assume that E is normalized such that $|E^2| = u = U/U_s$. In addition, the absorption step is derived from discretizing (4):

$$u_{j+1} = u_j \left[1 + \frac{\exp(-u_j) - 1}{u_j} \sigma n_0 \Delta z \right]. \quad (13)$$

Approximating the absorption term in (12) with (13) gives:

$$\exp \left[ik_0 \frac{\delta n(x, y, z_j)}{n_0} \Delta z \right] = \sqrt{1 + \frac{\exp(-|E_j^2|) - 1}{|E_j^2|} \sigma n_0 \Delta z}. \quad (14)$$

The simulation results for two beams with a peak fluence of $u_0 = 1500$ and $r \approx 4\%$ and $r \approx 10\%$, respectively, are shown in Fig. 3. The first pinhole has a triple product of $\beta = 50$. About 96% of the main beam and 2% of the side lobes are transmitted, corresponding to a noise attenuation of $\Gamma \approx 48$. The second pinhole has a triple product of $\beta = 125$. In this case, about 92% of the main beam and 6% of the side lobes are transmitted, corresponding to $\Gamma \approx 15$. If this were a 266 nm probe beam cleaned by ozone (i.e. $\sigma \approx 10^{-17}$ cm²/molecule at 1 atm, 293 K [15], $U_s \approx 75$ mJ/cm²), the triple products would correspond to a 5% ozone mixture and 4 cm and 10 cm propagation distances for the two pinholes. In comparison, the Rayleigh length is about 8.5 cm for 1 mrad divergence as used in our simulations.

According to (8) and (9), the transmission and attenuation would have been $T_0 \approx 97\%$ and $\Gamma \approx 10$ for the

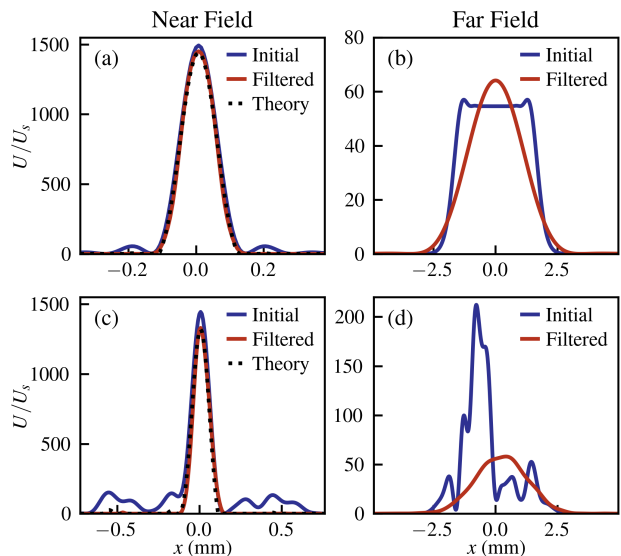


FIG. 3. Simulation results: (a) and (b) start with a super-Gaussian beam of order 5 ($r \approx 4\%$) and the triple product is $\beta = 50$; (c) and (d) apply an additional noise on top of the previous profile ($r \approx 10\%$) and the triple product is $\beta = 125$. For both beams, the divergence is 1 mrad and the peak fluence is $u_0 = 1500$ at the focal plane. The left panels show the beam profiles at the entrance and exit of the gas pinhole. The dotted lines are predictions based on (5). The right panels show the initial and filtered profiles far from the gas optic.

first setup and $T_0 \approx 92\%$ and $\Gamma \approx 4$ for the second one. The discrepancy may be due to neglecting diffraction in propagation and approximating energy contained by different modes with a single peak value. Nonetheless, the model is sufficient for suggesting parameters that can produce noticeable spatial cleaning effects. The discrepancy may also diminish as the Rayleigh length becomes much longer than the gas pinhole.

We further demonstrated this process experimentally with the setup in Fig. 1. The probe was created by frequency quadrupling a 1064 nm beam from a Q-switched Nd:YAG laser (Spectra-Physics PIV-400) via temperature-controlled DKDP and KDP crystals. The 266 nm probe contained an initial energy of 4.2 ± 0.1 mJ and had a full width at half maximum (FWHM) pulse duration of 5 ns. The beam was focused into an ozone-oxygen mixture flowing in a 3 cm wide aluminum tube with a 750 mm plano-convex lens followed by a 1000 mm plano-convex lens to achieve a long effective focal length. The diameter of the focal spot was around 0.84 mm in the gas. The ozone was produced by a corona-discharge-based ozone generator (Oxidation Technologies VMUS-4). The triple product was measured based on the linear absorption of a weak UV probe and reached up to 8.1 ($\sim 1.4\%$ O₃). The first row in Fig. 4 shows the spatial profiles of the beam with ozone off and at three different ozone concentrations, imaged by sending the beam directly to a CMOS camera (Alvium G5-812 UV). The second row shows the Fourier spectra of the profiles. The

high-frequency components were effectively suppressed as we increased the ozone concentration. Based on the Fourier spectra, the initial beam had a noisiness of $r \approx 0.24\%$. The gas pinhole delivered 86% transmission and 1.4 attenuation at $\beta = 1.3$, 78% transmission and 4.2 attenuation at $\beta = 4.7$, and 76% transmission and 8.1 attenuation at $\beta = 8.1$. The performance was likely limited by the extremely poor focal spot quality of the original beam, preventing complete cleaning with a single 3 cm ozone pinhole.

The experimental results demonstrate that ozone pinholes can significantly improve the spatial quality of an aberrated UV beam. In addition, we expect better temporal contrast since weaker prepulses will also be suppressed. The gas pinhole can be scaled to larger laser systems. For example, at $r = 2\%$ and $u_0 = 10^4$, a gas pinhole with $\beta = ru_0 = 200$ can deliver $t_0 = 98\%$ and $\gamma \approx 280$. The triple product can be achieved using a 5% ozone mixture at 1 atm, 293 K and an 8 cm long pinhole. Consider applications involving lasers at 248 nm or 266 nm ($U \approx 750 \text{ J/cm}^2$). The normalized fluence corresponds to a 500 mJ beam with a central waist of $w_0 \approx 0.15 \text{ mm}$, or a 50 J beam with a central waist of $w_0 \approx 1.5 \text{ mm}$. Scaling to kilojoule- and megajoule-class lasers without exceeding the damage thresholds or using extremely long focal lengths could be achieved with cylindrical lenses or mirrors that focus the beam in one axis and defocus in the other. Spatial modes in different directions will then be cleaned separately.

Finally, the gas pinhole can be adapted to lasers at different wavelengths, especially those in the visible and ultraviolet regimes. A non-exhaustive list of gases potentially suitable for different wavelengths is summarized in Table I. In the mid- and far-infrared regime, greenhouse gases including carbon dioxide and water vapor have particularly high absorption cross-sections, although it is unclear whether they will exhibit similar behavior for cleaning pulses. Since the device is insensitive to the pointing of the lasers, a multi-pass spatial filter can be built to achieve a longer effective attenuation distance and allow

the use of gases with smaller cross-sections.

TABLE I. **Gases suitable for filtering at different wavelengths.**

Gas	λ (nm)	$10^{20} \times \sigma$ ($\text{cm}^2/\text{molecule}$)	U_s (mJ/cm^2)
NH ₃	193	2000 [16]	51
O ₃	248	1080 [17]	74
O ₃	266	968 [17]	77
ClO ₂	351	1275 [17]	44
NO ₂	351	47 [18]	1204
NO ₂	532	16 [18]	2334

In conclusion, we have developed a gas-based spatial filter using saturated absorption in ozone and studied its performance with an analytic model, numerical simulations, and experiments. The results show significantly improved spatial quality of a 266 nm beam after focusing through a 3 cm 1.4% ozone-oxygen mixture, suggesting a method for building alignment-insensitive and damage-resistant pinholes for high-repetition-rate high-energy lasers.

Funding. This work was partially supported by NNSA Grant DE-NA0004130, NSF Grant PHY-2308641, and the Lawrence Livermore National Laboratory LDRD program (24-ERD-001).

Acknowledgments. Lawrence Livermore National Laboratory is operated by Lawrence Livermore National Security, LLC, for the U.S. Department of Energy, National Nuclear Security Administration under Contract DE-AC52-07NA27344.

Disclosures. Work at Stanford has been supported in part by Xcimer Energy LLC.

Data availability. Data underlying the results presented in this paper are not publicly available at this time but may be obtained from the authors upon reasonable request.

-
- [1] J. M. Auerbach and V. P. Karpenko, Serrated-aperture apodizers for high-energy laser systems, *Applied Optics* **33**, 3179 (1994).
 - [2] J. Hunt, P. Renard, and W. Simmons, Improved performance of fusion lasers using the imaging properties of multiple spatial filters, *Applied Optics* **16**, 779 (1977).
 - [3] A. Potemkin, T. Barmashova, A. Kirsanov, M. Martyanov, E. Khazanov, and A. Shaykin, Spatial filters for high-peak-power multistage laser amplifiers, *Applied Optics* **46**, 4423 (2007).
 - [4] R. W. Boyd, S. G. Lukishova, and Y. R. Shen, *Self-focusing: Past and present: Fundamentals and prospects* (Springer, 2009).
 - [5] J. E. Murray, D. Milam, C. D. Boley, K. G. Estabrook, and J. A. Caird, Spatial filter pinhole development for the National Ignition Facility, *Appl. Opt.* **39**, 1405 (2000).
 - [6] S. Szatmári, Z. Bakonyi, and P. Simon, Active spatial filtering of laser beams, *Optics Communications* **134**, 199 (1997).
 - [7] M. R. Edwards, N. M. Fasano, T. Bennett, A. Griffith, N. Turley, B. M. O'Brien, and J. M. Mikhailova, A multi-terawatt two-color beam for high-power field-controlled nonlinear optics, *Optics Letters* **45**, 6542 (2020).
 - [8] J. Kato, I. Yamaguchi, and H. Tanaka, Nonlinear spatial filtering with a dye-doped liquid-crystal cell, *Optics Letters* **21**, 767 (1996).
 - [9] A. Penzkofer and W. Fröhlich, Apodizing of intense laser beams with saturable dyes, *Optics Communications* **28**, 197 (1979).
 - [10] S. Sinha, K. Dasgupta, S. Sasikumar, and S. Kundu, Saturable-absorber-based spatial filtering of high-power laser beams, *Applied Optics* **45**, 4947 (2006).

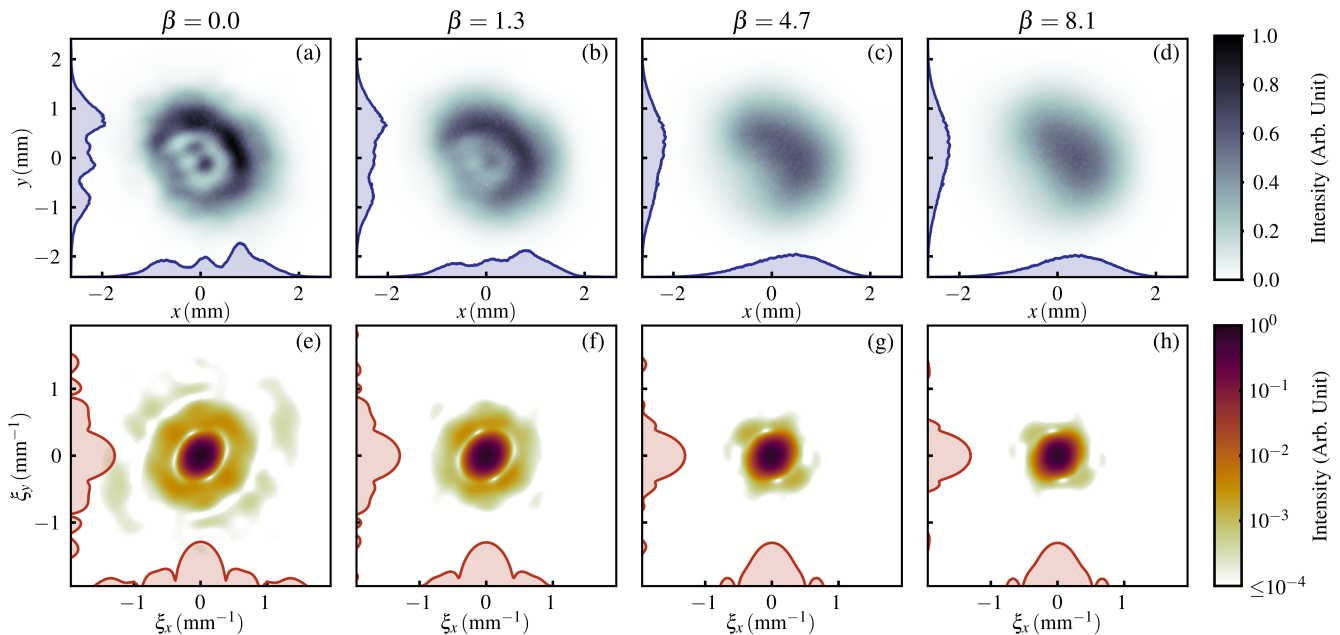


FIG. 4. Experimental results. (a)-(d). Spatial profile of the beam cleaned by a gas pinhole at four different triple products, adjusted by changing the ozone concentration. (e)-(f). Fourier spectra of the spatial profiles in the first row in logarithmic scale. The horizontal and vertical shaded curves show the central profile of the images.

- [11] Y. Michine and H. Yoneda, Ultra high damage threshold optics for high power lasers, *Communications Physics* **3**, 24 (2020).
- [12] P. Michel, L. Lancia, A. Oudin, E. Kur, C. Riconda, K. Ou, V. M. Perez-Ramirez, J. Lee, and M. R. Edwards, Photochemically induced acousto-optics in gases, *Physical Review Applied* **22**, 024014 (2024).
- [13] A. E. Siegman, *Lasers* (University Science Books, 1986).
- [14] P. Michel, *Introduction to laser-plasma interactions* (Springer Nature, 2023).
- [15] D. Daumont, J. Brion, J. Charbonnier, and J. Malicet, Ozone UV spectroscopy I: Absorption cross-sections at room temperature, *Journal of Atmospheric Chemistry* **15**, 145 (1992).
- [16] B.-M. Cheng, H.-C. Lu, H.-K. Chen, M. Bahou, Y.-P. Lee, A. M. Mebel, L. Lee, M.-C. Liang, and Y. L. Yung, Absorption cross sections of NH₃, NH₂D, NHD₂, and ND₃ in the spectral range 140-220 nm and implications for planetary isotopic fractionation, *The Astrophysical Journal* **647**, 1535 (2006).
- [17] J. Burkholder, S. Sander, J. Abbatt, J. Barker, C. Cappa, J. Crouse, T. Dibble, R. Huie, C. Kolb, M. Kurylo, *et al.*, *Chemical kinetics and photochemical data for use in atmospheric studies; evaluation number 19*, Tech. Rep. (Pasadena, CA: Jet Propulsion Laboratory, California Institute of Technology, 2020).
- [18] K. Bogumil, J. Orphal, T. Homann, S. Voigt, P. Spietz, O. Fleischmann, A. Vogel, M. Hartmann, H. Kromminga, H. Bovensmann, *et al.*, Measurements of molecular absorption spectra with the sciamachy pre-flight model: instrument characterization and reference data for atmospheric remote-sensing in the 230–2380 nm region, *Journal of Photochemistry and Photobiology A: Chemistry* **157**, 167 (2003).